# Dissipative dynamics of a solid-state qubit coupled to surface plasmons: From non-Markov to Markov regimes

A. Gonzalez-Tudela,[1,*] F. J. Rodríguez,[2] L. Quiroga,[2] and C. Tejedor[1]
[1]*Física Teórica de la Materia Condensada, Universidad Autónoma de Madrid, Madrid 28049, Spain*
[2]*Departamento de Física, Universidad de los Andes, A.A. 4976 Bogotá, Colombia*
(Received 1 June 2010; published 30 September 2010)

We theoretically study the dissipative dynamics of a quantum emitter placed near the planar surface of a metal supporting surface-plasmon excitations. The emitter-metal coupling regime can be tuned by varying some control parameters such as the qubit-surface separation and/or the detuning between characteristic frequencies. By using a Green's-function approach jointly with a time-convolutionless master equation, we analyze the non-Markovian dissipative features on the qubit time evolution in two cases of interest: (i) an undriven qubit initially prepared in its excited state and (ii) the evolution toward a steady state for a system driven by a laser field. For weak to moderate qubit-metal coupling strength, and on time scales large compared to the surface plasmon oscillation time, a Markovian approximation for the master-equation results to be adequate to describe the qubit main optical properties: surface enhancements of rate emission, optical spectra, and time-dependent photon-photon correlation functions. The qubit decay shows a crossover passing from being purely dissipative for small qubit-surface distances to plasmon emission for larger separations.

DOI: 10.1103/PhysRevB.82.115334 PACS number(s): 42.50.Nn, 42.50.Ex, 73.20.Mf

## I. INTRODUCTION

Surface plasmons (SPs) on metals, a topic extensively studied from many years ago,[1,2] has recently received a strongly renewed attention due to significant advances in new experimental capabilities and numerical developments.[3,4] Great attention has been focused on the emerging field of quantum plasmonic with the goal of making devices for quantum information processing[5,6] as single-photon transistor[7] or lasers.[8] As a requisite for this goal, a lot of effort has been devoted to get coherent coupling between plasmons and a quantum emitter made of a solid-state qubit (SSQ) as, for instance, a quantum dot, a single nitrogen vacancy (NV) center or a single molecule among others.

Strong coupling signatures of SSQ and SP have been experimentally observed both in spectroscopic as well as in time-resolved studies. In spectroscopy, the anticrossing between exciton and plasmon features in optical spectra have already been reported in systems such as organic semiconductors,[9] organic molecules placed in subwavelength hole arrays,[10] metallic nanowires,[11] hybrid metal-semiconductor nanostructures,[12] and even in carbon nanotubes.[13] These anticrossings have been claimed to be a manifestation of strong coupling between SSQ and SP. On the other hand, ultrafast time-resolved signatures of strong coupling in SSQ-SP systems have also been reported. An enhancement of several orders of magnitude for the spontaneous emission rate in a time-resolved photoluminescence measurement on a InGaN heterostructure close to a silver thin layer has been reported.[14,15] Additionally, recent experiments which operate simultaneously with both Raman and fluorescence signals coming from a single molecule in very close proximity to a metal surface have allowed the indirect measurement of ultrafast ($\sim$25 fs) dynamical features in such SSQ-SP system.[16]

On the theoretical side, some progress has been made to understand SSQ-SP coupling in different geometries using different approaches. The first attempts were devoted to computing the spontaneous emission rate enhancement of an atom near an absorbing surface as given by the atom self-energy in a near-field limit.[17] More recently, a hydrodynamic model[18] has been used to study a single molecule coupled to metallic nanoparticles. A transfer-matrix method has also been used for simulating attenuated-reflection experiments.[19] There are also some other interesting related works focused in the surface-enhanced Raman scattering of quantum emitters close to metallic nanoparticles,[20] dielectric spheroids,[21] or other more complex metallic structures.[22–24] However, the experimental setup which has risen the highest interest has been the quantum emitter coupled to a metallic nanowire,[11,25] where the generation of a single optical plasmon can be achieved. Several theoretical studies on this system have considered the full quantum behavior of plasmon modes.[26–28] In particular, some attention has been devoted[27] to non-Markovian effects that can be important in the SSQ-nanowire system because the spectral density $J(\omega)$ (carefully discussed in the present work) is highly structured due to a divergence at the edge of the SP density of states.

An open quantum system strongly coupled to a reservoir displays a complex dynamics which, in general, requires a description beyond simple Markovian theories.[29,30] In order to clarify the relevance of non-Markovian effects in SSQ-SP systems, we concentrate in a quantum emitter close to a planar surface of a dissipative metal, a system conceptually simpler than wires because it only has a single band of plasmons with a density of states having a singularity at a frequency $\omega_{sp}$. We study the properties of the light emitted by the system depicted in Fig. 1: a SSQ close to the planar metallic surface which supports a plasmon field as well as some dissipation mechanism. Strong SSQ-SP coupling could be expected when the qubit-surface distance is small compared with a typical length scale as, for instance, the wavelength of the emitted light. In order to understand the fundamental mechanisms of SSQ-SP strong coupling, we restrict our-

 

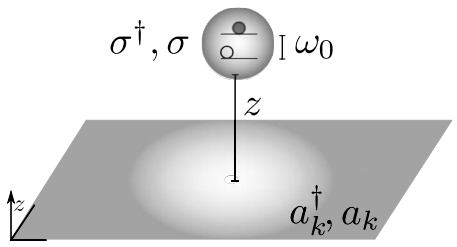


FIG. 1. Schematic view of the system: a SSQ, with characteristic frequency $\omega_0$, is placed at a distance $z$ of an infinite planar metallic surface.

selves to consider just a single quantum emitter. However, collective effects of many emitters coupled to the same plasmon field have been recently proposed[31] as responsible for the detection of the Rabi vacuum splitting in these systems.

We start by analyzing non-Markovian features in the SSQ-SP optical features by using a time-convolutionless (TCL) approach.[32] We show that SSQ-SP dissipative evolution is determined by the rapidly varying structure of the reservoir spectral function at a frequency close to $\omega_{sp}$ on the order of a few electron volts in a normal metal. Therefore, the time scale for non-Markovian effects reduces, at most, to a few hundreds times per electron volt, i.e., typical times under a picosecond. Consequently, we conclude that the observation of non-Markovian signatures in SSQ-SP systems made with normal metals will indeed demand experimental set ups at the edge front of present state-of-the-art ultrafast technology. Beyond this short-time scale, rate emissions stay constant and a Markovian approach becomes adequate for computing population dynamics, optical spectrum, and second-order coherence function. Here, both a Markovian and a non-Markovian analysis are applied to a SSQ-SP system under two different excitation schemes: first, we analyze the spontaneous emission of a SSQ initially prepared in the excited state. Second, the time evolution of a SSQ initially in its ground state and driven by means of a coherent laser field up to a stationary state is studied.

We take $\hbar=1$ along this paper which is organized as follows: in Sec. II we introduce the Green's tensor of the layered system and study its main properties, in particular, the spectral density function. In Sec. III the time-convolutionless method is briefly reviewed and the non-Markovian effects on the SSQ-SP system dynamics are considered. In Sec. IV we use the Markovian limit to calculate the optical properties of the system. Finally, in Sec. V we summarize our results and draw some conclusions.

## II. GREEN'S TENSOR AND SPECTRAL DENSITY

Electrodynamics of a dissipative medium is described by the Green's tensor $\hat{\mathbf{G}}(\mathbf{r},\mathbf{r}',\omega)$ which satisfies the Maxwell equation. We study the system depicted in Fig. 1: a SSQ in the upper-half space is embedded within a dielectric matrix with a dielectric function that can be taken as real and constant, $\epsilon_1$, in the range of frequencies of interest. In the lower half space, $z<0$, a dissipative metal is characterized by a complex dielectric function $\epsilon_2(\omega)$ that we take in a renormalized Drude approximation,

$$\epsilon_2(\omega)=\epsilon_\infty\left[1-\frac{\omega_p^2}{\omega(\omega+i\gamma_p)}\right]. \tag{1}$$

$\epsilon_\infty$ is the high-frequency limit of the metal dielectric function, $\omega_p$ is the bulk plasmon frequency, and $\gamma_p$ is the Landau damping constant.

The Green's tensor for this layered geometry has two contributions, $\hat{\mathbf{G}}(\mathbf{r},\mathbf{r}',\omega)=\hat{\mathbf{G}}_0(\mathbf{r},\mathbf{r}',\omega)+\hat{\mathbf{G}}_R(\mathbf{r},\mathbf{r}',\omega)$, the direct or free-space solution and the reflection contribution coming from its interaction with the materials,[2,32] with on-site $zz$ component,

$$G_{R,zz}(\mathbf{r},\mathbf{r},\omega)=-\frac{c^2}{4\pi\omega^2}\int_0^\infty dq\frac{q^3}{\kappa_1(q,\omega)}\times\left[\frac{\epsilon_1\kappa_2(q,\omega)-\epsilon_2(\omega)\kappa_1(q,\omega)}{\epsilon_1\kappa_2(q,\omega)+\epsilon_2(\omega)\kappa_1(q,\omega)}\right]e^{-2\kappa_1(q,\omega)z}, \tag{2}$$

where $\kappa_i(q,\omega)=\sqrt{q^2-\epsilon_i(\omega)(\omega/c)^2}$ for $i=1,2$. The components $G_{R,xx}, G_{R,yy}$ are also nonzero,[2,33] however we do not write them explicitly because they are not necessary in this work.

All the parameters of the absorbing medium relevant to the SSQ dissipative dynamics appear in the Green's tensor $\hat{\mathbf{G}}(\mathbf{r}_Q,\mathbf{r}_Q,\omega)$, where $\mathbf{r}_Q$ denotes the SSQ location. The action of the absorbing medium on a SSQ with dipole moment $\mathbf{p}$, is completely described by the spectral density

$$J(\omega)=\frac{1}{\pi\epsilon_0}\mathbf{p}\cdot\left\{\frac{\omega^2}{c^2}\mathrm{Im}[\hat{\mathbf{G}}(\mathbf{r}_Q,\mathbf{r}_Q,\omega)]\right\}\cdot\mathbf{p}, \tag{3}$$

which is related with the qubit-environment coupling $g(\omega)$ and the density of states of the environment $\rho(\omega)$ by means of $J(\omega)=g^2(\omega)\rho(\omega)$. In order to compute the spectral function of a representative system, we use parameters for silver in the range of frequencies of interest where $\omega_p=3.76$ eV, $\epsilon_\infty=9.6$, and $\gamma_p=0.03\omega_p$,[34] while for the dielectric constant at the upper-half space we take $\epsilon_1=5$. Since the density of states has a singularity at $\omega_{sp}=\omega_p\sqrt{\epsilon_\infty/(\epsilon_1+\epsilon_\infty)}=0.81\omega_p$ non-Markovian effects associated with the structured reservoir can be expected to occur around that inverse frequency. Thus, we consider a SSQ with a dipole oriented along the $z$ direction and an energy splitting $\omega_0$ slightly detuned with respect to the singularity at the SP edge $\omega_{sp}$. In particular, we calculate $J(\omega)$ for $\Delta=\bar{\omega}_{sp}-\bar{\omega}_0=0.1$, where the frequencies have been normalized to the bulk plasmon frequency $\bar{\omega}_{sp}=\omega_{sp}/\omega_p$ and $\bar{\omega}_0=\omega_0/\omega_p$.

In Fig. 2 we plot, for different values of the qubit-surface renormalized separation $\bar{z}=z\omega_p/c$, the spectral density in units of the spontaneous decay rate of the SSQ in free space $\gamma_0=\omega_0^3p^2/3\pi\epsilon_0c^3$. Two main results can be identified: (i) a strong reduction in $J(\omega)$ when the qubit gets farther from the surface. This is a consequence of the exponential reduction in the coupling, as a function of $z$, as indicated in Eq. (2).

(ii) For small separations $J(\omega)$ is highly structured presenting a strong peak close to the frequency $\omega_{sp}$ (vertical line in Fig. 2). This is a consequence of the singularity of the

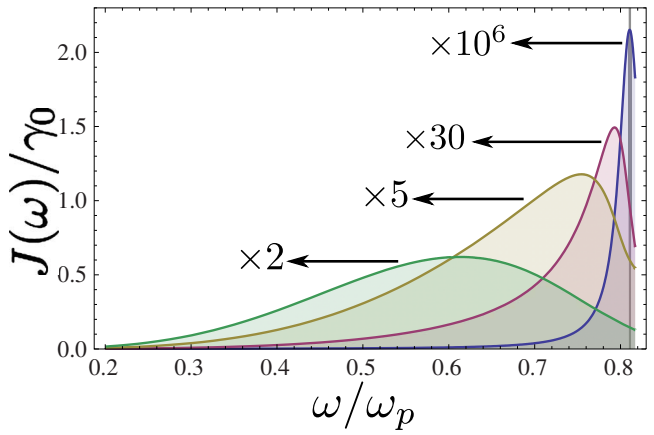


FIG. 2. (Color online) Spectral density $J(\omega)/\gamma_0$ for a detuning $\Delta=\bar{\omega}_{sp}-\bar{\omega}_0=0.1$ plotted for different qubit-surface separations: $\bar{z}=\omega_p z/c=0.01$ (blue), 0.32 (purple), 0.64 (yellow), and 1.42 (green). Notice that as far as the SSQ approaches the surface, the spectral density increases in roughly 6 orders of magnitude.

density of SP states at small detunings $\Delta$. For increasing separation, $J(\omega)$ becomes much smoother and a reduced maximum separates from $\omega_{sp}$.

## III. TIME-CONVOLUTIONLESS METHOD AND NON-MARKOVIAN EFFECTS

The spectral density for the SSQ-SP system computed within a purely classical scheme, can be used within a quantum framework describing the dissipative dynamics of an open quantum system. As it is well known, when the time correlation between the system and the environment decay much faster than the characteristic inverse dissipation rate, memory effects can be neglected in the so-called Markovian approximation, and the observables of the system are given by analytical expressions. However, this time scale does not represent the only one relevant to determine the system's evolution. When the environment correlation time is longer than the inverse rate of the system-bath coupling, distinct physics can arise at very short times. A SSQ in close proximity to a dissipative metal surface supporting SP modes sees a highly structured reservoir to which might be strongly coupled. Thus, one can expect non-Markovian effects to be significant in the qubit time evolution. Many works[27,32,35–46] have been devoted to treat this problem at different levels of precision and sophistication. Here, we chose to work within a TCL framework[32] to capture non-Markovian effects to the lowest order in the SSQ-SP coupling strength. This method has already been applied to consider the spontaneous decay of a two-level system coupled to a general structured reservoir.[32] For SSQ-SP systems, the strong variation in $J(\omega)$ occurring for frequencies close to $\omega_{sp}$, implies that dynamical features in time scales from femtoseconds to picoseconds are expected.

### A. Time-convolutionless method

What is of interest for us of the TCL method can be sketched as follows.[32] It consists in transforming the typical non-Markovian integrodifferential equation for the reduced density matrix into a local in time evolution equation by making use of a power expansion technique of the Nakajima-Zwanzig type. As a result, a master equation for a qubit is obtained with time-dependent decay rate $\gamma(t)$ and Lamb shift $S(t)$,

$$\frac{d\rho(t)}{dt}=\frac{i}{2}S(t)[\rho(t),\sigma^+\sigma^-]+\frac{\gamma(t)}{2}\times[2\sigma^-\rho(t)\sigma^+-\sigma^+\sigma^-\rho(t)-\rho(t)\sigma^+\sigma^-]. \quad (4)$$

Time-dependent rates can be calculated within a perturbative expansion. In order to calculate them, a first step is to Fourier transform the spectral density,

$$f(t)=\int d\omega J(\omega)e^{i(\omega_0-\omega)t}. \quad (5)$$

The lowest order non-Markovian effects, i.e., the so-called post-Markovian behavior, are contained in the second-order contributions to $\gamma(t)$ and $S(t)$ given by

$$\gamma_2(t)=\frac{1}{2}\int_0^t dt_1\Re f(t-t_1), \quad (6)$$

$$S_2(t)=\frac{1}{2}\int_0^t dt_1\Im f(t-t_1), \quad (7)$$

where $\Re$ and $\Im$ denote real and imaginary parts, respectively.

### B. SSQ spontaneous decay

We start by considering the situation where an undriven SSQ is prepared in its excited state from which decays emitting a photon to the vacuum or to the SP field. There are two possible situations depending on the sign of the detuning $\Delta$ between SP $\bar{\omega}_{sp}$ and the SSQ $\bar{\omega}_0$ renormalized frequencies. The time evolution of the excited state population is given by[32]

$$n_1(t)=n_1(0)e^{-\int_0^t\gamma_2(s)ds} \quad (8)$$

with $n_1(0)=1$ and the decay rate obtained from Eq. (6).

At this stage, we want to analyze the importance of memory effects. Therefore, in the calculations reported in this section we do not include the free-space part of the Green's tensor, which involves a much slower dynamics than the one associated to the reflection contribution $\hat{\mathbf{G}}_R$, as given in Eq. (2).

Figure 3 shows $n_1(t)$ for different positive detunings, i.e., when the SSQ is resonant with the continuum stripe of SP modes $(0<\omega<\omega_{sp})$. In order to have a highly structured reservoir, we have taken a small qubit-surface separation, $\bar{z}=0.055$ (very close to the blue line spectral density in Fig. 2). For large detuning $\Delta=0.5$, $\gamma_2(t)$ oscillates around a constant (Markovian) value. At some time intervals, $\gamma_2(t)$ takes on negative values, a fact that tends to slow down the decay of the excited state population. Physically, this behavior can be understood as due to the backaction of the reservoir on the SSQ re-exciting it. When the SSQ splitting energy gets

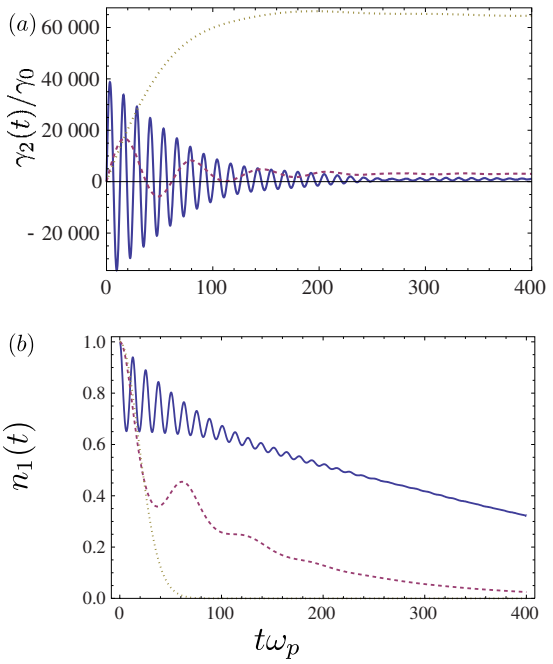


FIG. 3. (Color online) (a) Decay rate and (b) population of the excited state of a SSQ located at $\bar{z}=0.055$ from the planar surface. Different lines correspond to different detunings from the SP frequency: $\Delta=\bar{\omega}_{sp}-\bar{\omega}_0=0.5$ (solid blue), 0.1 (dashed purple), and 0.01 (dotted yellow).

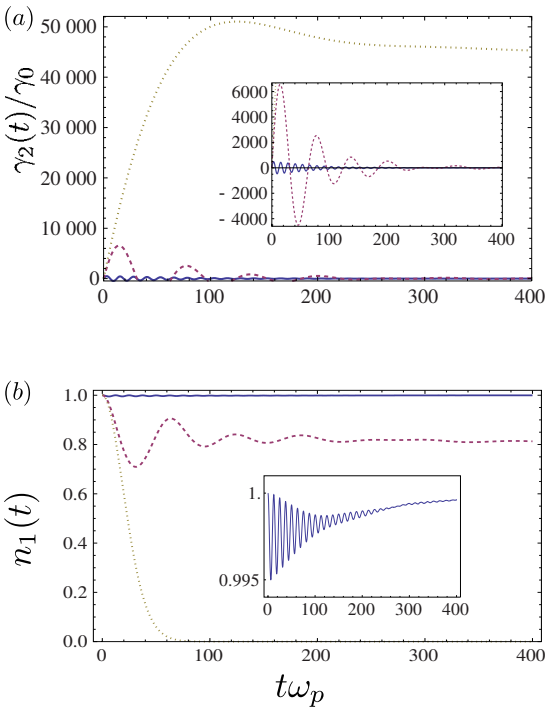


FIG. 4. (Color online) Decay rate and population of the excited state for a SSQ placed at $\bar{z}=0.055$ from the planar surface. The different lines correspond to different detunings: $\Delta=\bar{\omega}_{sp}-\bar{\omega}_0=-0.5$ (solid blue), $-0.1$ (dashed purple), and $-0.01$ (dotted yellow). Inset in (a) corresponds to a zoom of the decay rate for the first two values of $\Delta$ while inset in (b) corresponds to a zoom to population of the excited state at short times for $\Delta=-0.5$. Including the effect of free-space emission ($\gamma_0$) produces a decay of $n_1$ in a time scale much larger than that of the figure.

closer in resonance with the top SP energy, e.g., $\Delta=0.1$, the oscillations slow down, the envelope of the oscillatory decay rate becomes smaller and the negative parts of the decay rate $\gamma_2(t)$ tend to vanish producing only few oscillations before the spontaneous decay becomes almost exponential. For further smaller detunings, e.g., $\Delta=0.01$, the SSQ frequency becomes close to a singularity in the SP density of states. The decay rate modifies completely its behavior, increasing considerably its value and just oscillating slightly around a large positive value. The SSQ-SP coupling strength, for the smallest detuning, is becoming so large that a perturbative approach like the second-order TCL method should fail to render reliable results, as reflected in the monotonous decay of the SSQ excited state population with no oscillatory structure [see Fig. 3(b)]. Physically, the transfer of the SSQ energy to the SP field is very fast in this small detuning case, bringing the SSQ to its ground state with coherence effects in a very short-time scale. More elaborated methods are required to explore this ultra-strong-coupling (SC) regime but this is certainly beyond the scope of the present work.

On the other hand, a physically different situation occurs for negative detunings, i.e., when the SSQ energy falls within the gap where no SP states exist. Figure 4 is similar to Fig. 3 with the same $\bar{z}$ and detunings with just a change in sign with respect to the ones in Fig. 3. When $\omega_0$ is far above the edge of the SP dispersion, the SSQ basically remains in its excited state as the spectral density for these energies is practically zero, so there are no accessible SP modes to which decay into. Nevertheless, as shown in the inset of Fig. 3, one may observe some non-Markovian oscillations for very short times. When the SSQ energy is tuned closer in resonance with $\bar{\omega}_{sp}$, e.g., $\Delta=0.1$, a very interesting phenomenon occurs: the emitter undergoes the so-called fractional decay in which the population tends to a finite, nonzero, value at long times. Including the effect of free-space emission ($\hat{\mathbf{G}}_0$) produces a decay of $n_1$ in a time scale ($\gamma_0^{-1}$) much larger than that of the figure. As the emission frequency is further scanned closer to the band edge, the behavior changes again dramatically: the decay rate, instead of oscillating around zero, oscillates slightly around a positive value, which results into an irreversible exponential decay.

A very important result must be drawn from all these results: the time scale of these non-Markovian effects is a few hundred times $\omega_p^{-1}$. For normal metals, this means times below 1 ps. Beyond that short-time scale, $\gamma_2$ becomes constant just at the value it takes in a Markovian description as discussed in the following Sec. IV.

### C. Coherently driven SSQ

After having studied the effect of the structured reservoir on the SSQ spontaneous emission, now we turn our attention to the case where the system is coherently driven by a laser field. The SSQ emits and absorbs photons simultaneously. The system can achieve a stationary state in which light absorbed from the laser ends being transferred to plasmons.

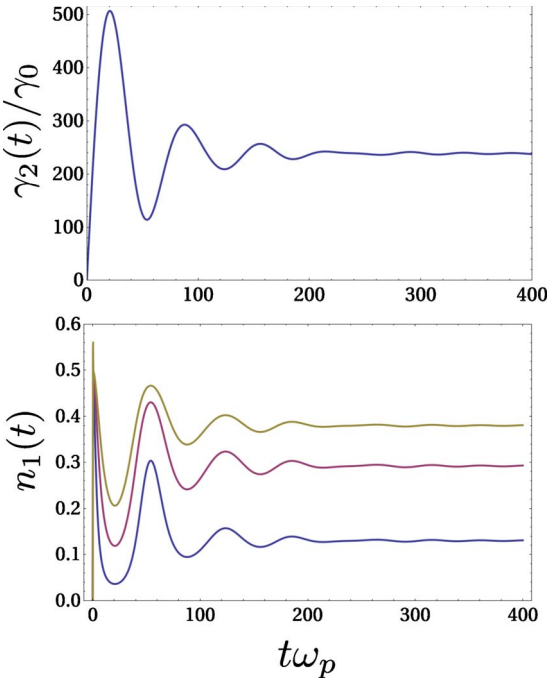


FIG. 5. (Color online) Decay rate and excited population of a SSQ placed at $\bar{z}=0.2$ with energy detuning $\Delta=\bar{\omega}_{sp}-\bar{\omega}_0=0.1$ and coherently driven by a laser in resonance with the SSQ. The different lines correspond to different laser intensities: $\Omega/\gamma_0=100$ (blue), 200 (purple), and 500 (yellow).

The laser can be treated as a classical field included in the, local in time, coherent part of the master Eq. (4) through the Hamiltonian $H_{\rm las}=\Omega(\sigma^+e^{i\omega_{\rm las}t}+e^{-i\omega_{\rm las}t}\sigma^-)/2$. The Rabi frequency $\Omega$ measures the strength of the coupling of the SSQ dipole with the laser field. The time evolution of the SSQ excited state population is obtained from the solution of Eq. (4) represented in a rotating frame at the laser frequency $\omega_{\rm las}$. $n_1(t)$ is plotted in Fig. 5, for the case of perfect resonance between the laser and the SSQ. We assume that $\gamma_2(t)$ remains unaffected by the laser field so that the main effect of the laser is to bring the system to a stationary state in a time scale which is similar to that of the spontaneous decay discussed in the previous section.

## IV. OPTICAL PROPERTIES IN THE MARKOV APPROXIMATION

The results of the previous section show that a SSQ presents significant non-Markovian effects in a time scale a couple of orders of magnitude larger than $\omega_p^{-1}$. Hereafter, we concentrate in the usual case of having a resolution in time larger than a picosecond. Then, the system can be described by a Markovian dynamics given by a master equation such as Eq. (4) but now with a Lamb shift $S=S_2(t\to\infty)$ and a constant decay rate $\gamma=\gamma_2(t\to\infty)$ including both the free space and the reflection contributions to the dissipative dynamics. Since the only effect of the Lamb shift is a constant energy shift, from now on we do not pay attention to it.

### A. Decay rate

The decay rate in the Markovian regime coincides with the long-time limit of $\gamma_2(t)$, $\gamma=\gamma_2(t\to\infty)$, allowing to identify $\gamma$ as simply the spectral function at the SSQ frequency,

$$\gamma=2\pi J(\omega_0)=\frac{2\omega_0^2}{\epsilon_0 c^2}\mathbf{p}\cdot\mathrm{Im}[\hat{\mathbf{G}}(\mathbf{r}_Q,\mathbf{r}_Q,\omega_0)]\cdot\mathbf{p}, \qquad (9)$$

where the two terms corresponding to the free space ($\hat{\mathbf{G}}_0$) and the reflection part ($\hat{\mathbf{G}}_R$) of the dissipative dynamics are included in $\hat{\mathbf{G}}$.

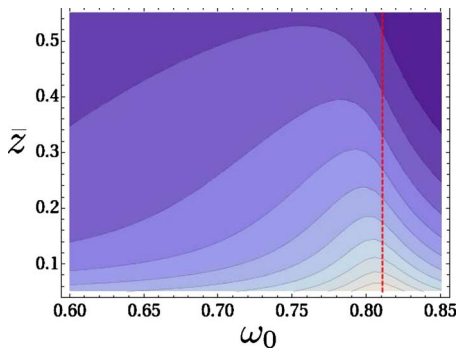


FIG. 6. (Color online) Surface-assisted decay rate $\log_{10}(\gamma/\gamma_0)$ given by Eq. (9) for a region of the $\bar{z},\bar{\omega}_0$ parameter space. The red dotted gridline marks the $\bar{\omega}_{sp}$ frequency. Lighter blues correspond to high values. Between the highest and the lowest values there are four orders of magnitude.

The SSQ decay rate to the SP reservoir of the metallic surface, $\gamma$, is shown in Fig. 6, in a parameter space $\{\bar{z},\bar{\omega}_0\}$, where lighter blues correspond to high decay rates with a variation in four orders of magnitude between the highest and the lowest values. In order to discuss these results, it is better to plot $\gamma$ vs the SSQ-interface distance $\bar{z}$ (in logarithmic scales) for different SSQ energies as depicted in Fig. 7. It is worth noticing two important features: first, at a large $\omega_0$ value the assisted decay rate is smaller than the vacuum one for a certain range of distances, due to the fact that the reflected part of the Green's tensor is interfering destructively with the direct one. This effect is evident when the SSQ frequency approaches $\omega_{sp}$ while it moves to larger separations $\bar{z}$, and it weakens, when $\omega_0$ is far from the SP band edge.

Second feature is even more important. When the SSQ-surface distance varies, the decay rate suffers a transition

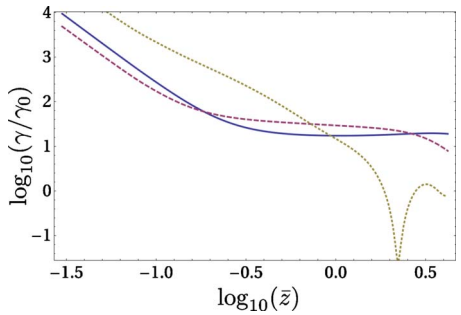


FIG. 7. (Color online) Logarithmic relative decay rate $\log_{10}(\gamma/\gamma_0)$ calculated with Eq. (9) as a function of $\log_{10}(\bar{z})$. The three curves correspond to different SSQ energies $\bar{\omega}_0=0.24$ (solid blue), 0.4 (dashed purple), and 0.76 (yellow dotted).

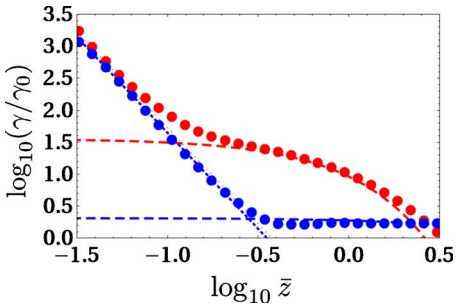


FIG. 8. (Color online) Logarithmic relative decay rate $\log_{10}(\gamma/\gamma_0)$ calculated with Eq. (9) as a function of $\log_{10}(\bar{z})$ with $\epsilon_1=\epsilon_\infty=1$ and $\gamma_p=\omega_p/500$. Two different SSQ energies are considered: $\bar{\omega}_0=0.2$ (blue circles, far from the SP edge) and 0.6 (red circles, close to the SP edge). Dashed lines denote the decay rates as predicted by a single pole approximation (SP contribution). Dotted lines correspond to metal losses as the emission of electron-hole pairs.

from a $1/z^3$ behavior to a much slower decrease. In order to understand the physics behind this behavior, we analyze the much simpler case $\epsilon_1=\epsilon_\infty=1$ and $\gamma_p=\omega_p/500$, i.e., a rate for losses one order of magnitude smaller than the one we have used in previous cases. Large dots in Fig. 8 depict the decay rate as calculated with the full Green's tensor for two different SSQ frequencies. At very short distances the decay rate is highly enhanced with respect to $\gamma_0$ and shows a $1/z^3$ dependence, which can be obtained (dotted lines in the figure) by means of a model which only contains nonradiative processes as the creation of electron-hole pairs in the metallic medium. A crossover to a different behavior occurs at a critical distance, which depends on the SSQ-SP detuning $\Delta$. Beyond this critical distance, a single plasmon pole approximation (dashed lines in the figure) in the Green's tensor in Eq. (9) is able to reproduce the numerical result with the complete Green's tensor. In other words, for separations beyond the crossover, the SSQ decay just produces the emission of surface plasmons while other metallic losses become negligible. In the case of the SSQ embedded in a dielectric or a metal with very large losses this crossover can be hindered by other physical effects such as those coming from local dissipative circulating currents.[28] As the SP channel contribution increases when the SSQ energy gets closer to the plasmon band edge, this crossover effect can be exploited in designing coherent plasmonic devices.[12]

### B. Spectrum and correlation functions

Hereafter, we consider the case in which the system is coherently driven by a laser so that the system reaches a stationary state with partial occupation of the two levels of the SSQ. The master equation in the rotating frame at the laser frequency, $\omega_{\rm las}$, is

$$\frac{d\rho(t)}{dt}=i\left\{\Delta\omega[\rho(t),\sigma^+\sigma^-]+\frac{\Omega}{2}[\rho(t),\sigma^++\sigma^-]\right\}$$
$$+\frac{\gamma}{2}[2\sigma^-\rho(t)\sigma^+-\sigma^+\sigma^-\rho(t)-\rho(t)\sigma^+\sigma^-] \quad (10)$$

with $\Delta\omega=\omega_0-\omega_{\rm las}$. The problem reduces to the study of the SSQ resonance fluorescence[47] near the planar surface of a dissipative metal. The vacuum resonance fluorescence has been widely studied in the literature in the case of resonant excitation for which an analytical solution for the population, spectrum, and second-order coherence function exists. Here, we extend such analysis to the nonresonant case and pay special attention to the effect of the SP reservoir. We present our analysis in the way the experiments can be performed either by tuning the laser resonantly with the SSQ energy and varying the laser intensity or by fixing the laser intensity and scanning the laser frequency. Figure 9 explores the former alternative whereas in Fig. 10 we consider the later one.

From the master Eq. (10) one may derive the equations of motion for the expectation values $\langle\sigma^+(t)\rangle$, $\langle\sigma^-(t)\rangle$, and $\langle\sigma^z(t)\rangle$ arriving to the well-known optical Bloch equations (OBEs). The steady-state solution for the excited state population is

$$\langle n_1\rangle_{ss}=\frac{\Omega^2}{(\gamma^2+4\Delta\omega^2+2\Omega^2)}. \quad (11)$$

In general, the OBE must be solved numerically in order to get the population dynamics $\langle n_1(t)\rangle$, except for the resonant case ($\Delta\omega=0$) for which an analytical solution exists,

$$\langle n_1(t)\rangle=\frac{\Omega^2}{\gamma+2\Omega^2}\times\left\{1-e^{-3\gamma t/4}\left[\cos(Rt)+\frac{3\gamma}{4R}\sin(Rt)\right]\right\}, \quad (12)$$

where $R=\sqrt{\Omega^2-\gamma^2/16}$, labeled as Rabi splitting at resonance,[48] is the parameter characterizing the strength of the effective coupling. There is a threshold for the laser intensity at $\Omega=\gamma/4$. For $\Omega$ below this threshold, the solutions are monotonically decaying functions of time so that the system is said to be in the weak-coupling (WC) regime. Above that threshold, the populations exhibit oscillations, and the system is said to be in the SC regime. In Fig. 9(a) we plot the real part of $R$ in the parameter space $\{\bar{z},\bar{\Omega}_0\}$. The bluest region corresponds to $\Re(R)=0$, which means that the Rabi splitting at resonance is purely imaginary and consequently the system is in the WC regime. For the regions in which blue becomes lighter, the values correspond to positive and higher values of $\Re(R)$.

In order to clarify these results, we show the population dynamics in Fig. 9(b) for three different points highlighted in part (a) of the same figure: the green curve corresponds to a configuration where the laser is weakly coupled to the system, so no oscillations are observed in the population. The red point corresponds to the region of transition from WC to SC where just one clear oscillation occurs before practically arriving to the steady state. Finally the blue point corresponds to a configuration where the laser is strongly coupled to the SSQ and several oscillations are observed before the steady state is achieved.

Another experimental alternative is to keep $\Omega$ constant and vary the laser frequency as it is plotted in Fig. 10. In this case, the laser is out of resonance and the Rabi splitting must be redefined as[48]

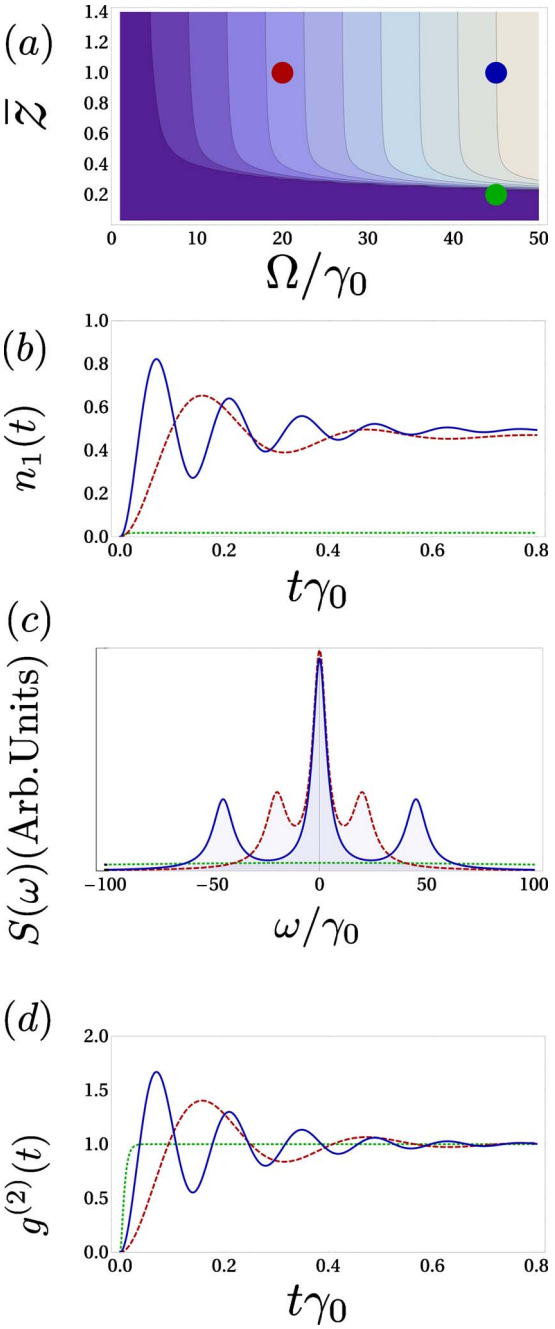


FIG. 9. (Color online) Optical properties of the SSQ-SP system. Panel (a) corresponds to the value of $\Re(R)$ in the parameter space $\{\bar{z},\bar{\Omega}_0\}$ in order to distinguish the strong- and weak-coupling regions. Panel (b) and (d) show the dynamics of the excited state population and the two-photon correlation function $[g^{(2)}(t)]$, respectively, for the three points plotted in panel (a), corresponding to values of $\gamma/\gamma_0=327$ for the red point and 7.7 for the other two. Panel (c) shows the qubit luminescence spectra for those three particular cases.

$$R_\Delta = \sqrt{\Omega^2 - \left(\frac{\gamma}{4} + i\Delta\omega\right)^2}. \tag{13}$$

Figure 10(a) shows $\Re R_\Delta$ in the parameter space $\{\bar{z},\Delta\bar{\omega}\}$. The population dynamics is shown in panel (b) of the same figure, where one can observe the transition from strong coupling (oscillations, solid blue) to weak coupling (monotonous in time, green dotted) for nonresonant excitation of the SSQ.

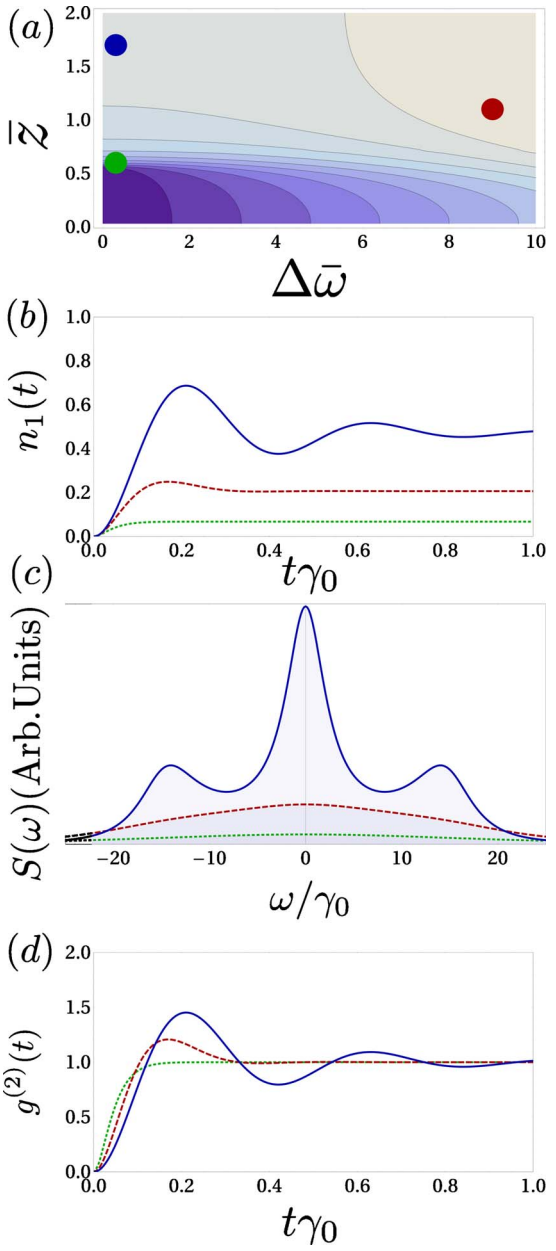


FIG. 10. (Color online) Optical properties of the SSQ-SP system. Panel (a) corresponds to the value of $\Re(R_\Delta)$ in the parameter space $\{\bar{z},\Delta\bar{\omega}\}$ to distinguish the strong- and weak-coupling regions. Panel (b) and (d) show the dynamics of the excited state population and the two-photon correlation function $[g^{(2)}(t)]$, respectively, for the three points plotted in panel (a), corresponding to values of $\gamma/\gamma_0=72$, 22, and 8 for the green, red, and blue points, respectively. Panel (c) shows the SSQ luminescence spectra for those three particular cases.

A clear manifestation of the transition from WC to SC appears in the optical spectrum at the stationary regime. It can be calculated through the Wiener-Khintchine formula,

$$S(\omega) = \frac{1}{\pi}\Re\int_0^\infty e^{i\omega\tau}\langle\sigma^+(t)\sigma^-(t+\tau)\rangle d\tau. \tag{14}$$

The calculation of the two-time correlator in Eq. (14) requires the use of the quantum regression theorem[47] by using the steady-state populations as initial values for the second time dynamics. In the resonance fluorescence problem there are always two main contributions to the spectra: the Rayleigh scattering coherent part and the one coming from the incoherent scattering. The former contribution is just a delta function at $\omega_0$ that we ignore in our results. We are mainly interested in the contribution coming from the inelastic scattering which is shown in Figs. 9(c) and 10(c) for the resonant and nonresonant cases, respectively. As it occurred with the population, under resonant excitation the spectrum admits an analytical expression,

$$S(\omega) \propto \left[\frac{\gamma/4}{\frac{\gamma^2}{4}+(\omega-\omega_0)^2} + \frac{3\gamma/16}{\frac{9\gamma^2}{16}+(\omega-\omega_0+\Omega)^2} + \frac{3\gamma/16}{\frac{9\gamma^2}{16}+(\omega-\omega_0-\Omega)^2}\right]. \tag{15}$$

In the WC regime (green point) $\Omega < \gamma/4$, the light emitted simply produces a Lorentzian curve peaked about $\omega_0$ with linewidth $\gamma/2$. For the intermediate regime (red point), on top of the Lorentzian peaked at the qubit frequency, some satellites start to appear at the laser Rabi frequency $\pm\Omega$. For a strong-driving field situation $\Omega > \gamma/4$ these two sidebands appear at frequencies $\omega = \omega_0 \pm \Omega$. For the nonresonant case, the threshold changes but the behavior remains qualitatively unaffected: even though the dressed state structure is slightly modified by the detuning, at the end, a triplet is obtained in the resonant case. The existence of this Mollow's triplet is a manifestation of the SC of the laser to the SSQ-SP system.

Another magnitude of experimental interest is the second-order coherence function,

$$g^{(2)}(\tau) = \frac{G^{(2)}(t,t+\tau)}{G^{(1)}(0)G^{(1)}(\tau)} \tag{16}$$

with correlation functions

$$G^{(2)}(t,t+\tau) = \langle\sigma^{(+)}(t)\sigma^{(+)}(t+\tau)\sigma^{(-)}(t+\tau)\sigma^{(-)}(t)\rangle,$$

$$G^{(1)}(t,t+\tau) = \langle\sigma^{(+)}(t)\sigma^{(-)}(t+\tau)\rangle. \tag{17}$$

We evaluate these magnitudes at the stationary state. In the resonant case, the second-order coherence function can be analytically expressed as

$$g^{(2)}(\tau) = 1 - e^{-3\gamma\tau/4}\left[\cos(R\tau) + \frac{3\gamma}{4R}\sin(R\tau)\right]. \tag{18}$$

It clearly exhibits photon antibunching: $g^2(0)=0$. Figure 9(d) shows $g^{(2)}$ for zero detuning for the three different points considered above for the other magnitudes. Apart from the antibunching, the case of SC shows a remarkable oscillatory behavior. Once more, qualitatively similar results are obtained with laser-SSQ detuning as shown in Fig. 10(d).

The main consequence to be drawn from Figs. 9 and 10 is that by pumping the SSQ with a tunable laser, and measuring spectra and second-order correlation functions, one can extract information about the SSQ coupling to the surface plasmon of the dissipative metal.

## V. SUMMARY

In this work we have studied the properties of the coupling of light with a SSQ, embedded in a dielectric, in the presence of a SP field supported in the interface between this dielectric matrix and a dissipative metal. Using a time-convolutionless approach, we provide a theoretical description of the non-Markovian features for this kind of systems and discuss its relevance in possible observations. In a spontaneous decay situation, different behaviors occur depending on both the sign and the absolute value of the SSQ-SP detuning: from a monotonous (almost exponential) decay for very small detunings, to population oscillations due to reabsorptions in the case of positive detuning. Even fractional decays can be observed, when negative detunings are present and the SSQ energy is not too close to the SP edge band.

In experimental situations, non-Markovian features can be hard to detect due to practical difficulties in getting the adequate time resolution. Therefore, we have also considered a Markov approximation to study the electrodynamics of the SSQ coupled to a reservoir of SP modes. The whole information of the planar metallic surface is embedded in the decay rate constant, which depends on both the SSQ frequency and distance to the surface. The excitation of the system by a laser allows the existence of a steady state as well as the analysis of different measurable properties of the SSQ-SP system as, for instance, surface enhancements of rate emission, optical spectra, and time-dependent photon-photon correlation functions. Our main result is that the qubit decay shows a crossover passing from being purely dissipative for small qubit-surface distances to plasmon emission for larger separations. As the SP emission channel increases when the SSQ energy gets closer to the plasmon band edge, this crossover effect can be exploited in designing coherent plasmonic devices. Our next task, beyond the scope of the present work, is to treat the plasmonic part of the system not as a reservoir but as an ingredient coherently coupled to one or more SSQs.[12]

## ACKNOWLEDGMENTS

Helpful discussions with F. J. Garcia-Vidal and L. Martin-Moreno are acknowledged. Work supported in part by the Spanish MEC Consolider-Ingenio2010 under Contracts No. QOIT-CSD2006-00019 and No. MAT2008-01555, and by the CAM under Contract No. S-0505/ESP-0200. A.G.-T. acknowledges funding from AP2008-00101 FPU grant of Spanish Education Ministry. L.Q. was partially supported by Faculty of Sciences-Research Funds 2009 (UniAndes). F.J.R. was partially supported by Banco de la Republica (Colombia).

*Corresponding author; alejandro.gonzalez@uam.es


[1] H. Raether, *Surface Plasmons* (Springer-Verlag, Berlin, 1988).
[2] L. Novotny and B. Hecht, *Principles of Nano-Optics* (Cambridge University Press, Cambridge, 2006).
[3] W. L. Barnes, A. Dereux, and T. W. Ebbesen, Nature (London) **424**, 824 (2003).
[4] F. J. Garcia-Vidal, L. Martin-Moreno, T. W. Ebbesen, and L. Kuipers, Rev. Mod. Phys. **82**, 729 (2010).
[5] D. E. Chang, A. S. Sørensen, P. R. Hemmer, and M. D. Lukin, Phys. Rev. Lett. **97**, 053002 (2006).
[6] D. E. Chang, A. S. Sørensen, P. R. Hemmer, and M. D. Lukin, Phys. Rev. B **76**, 035420 (2007).
[7] D. E. Chang, A. S. Sørensen, E. A. Demler, and M. D. Lukin, Nat. Phys. **3**, 807 (2007).
[8] R. F. Oulton, V. J. Sorger, T. Zentgraf, R.-M. Ma, L. Dai, G. Bartal, and X. Zhang, Nature (London) **461**, 629 (2009).
[9] J. Bellessa, C. Bonnand, J. C. Plenet, and J. Mugnier, Phys. Rev. Lett. **93**, 036404 (2004).
[10] J. Dintinger, S. Klein, F. Bustos, W. L. Barnes, and T. W. Ebbesen, Phys. Rev. B **71**, 035424 (2005).
[11] A. V. Akimov, A. Mukherjee, C. L. Yu, D. E. Chang, A. S. Zibrov, P. R. Hemmer, H. Park, and M. D. Lukin, Nature (London) **450**, 402 (2007).
[12] P. Vasa *et al.*, Phys. Rev. Lett. **101**, 116801 (2008).
[13] I. V. Bondarev, L. M. Woods, and K. Tatur, Phys. Rev. B **80**, 085407 (2009).
[14] A. Neogi, C.-W. Lee, H. O. Everitt, T. Kuroda, A. Tackeuchi, and E. Yablonovitch, Phys. Rev. B **66**, 153305 (2002).
[15] K. Okamoto, I. Niki, A. Scherer, Y. Narukawa, T. Mukai, and Y. Kawakami, Appl. Phys. Lett. **87**, 071102 (2005).
[16] C. M. Galloway, P. G. Etchegoin, and E. C. Le Ru, Phys. Rev. Lett. **103**, 063003 (2009).
[17] M. S. Yeung and T. K. Gustafson, Phys. Rev. A **54**, 5227 (1996).
[18] A. Trügler and U. Hohenester, Phys. Rev. B **77**, 115403 (2008).
[19] M. S. Tame, C. Lee, J. Lee, D. Ballester, M. Paternostro, A. V. Zayats, and M. S. Kim, Phys. Rev. Lett. **101**, 190504 (2008).
[20] P. Johansson, H. Xu, and M. Käll, Phys. Rev. B **72**, 035427 (2005).
[21] J. Gestern and A. Nitzan, J. Phys.: Condens. Matter **75**, 1139 (1981).
[22] V. Yannopapas and N. V. Vitanov, J. Phys.: Condens. Matter **19**, 096210 (2007).
[23] V. Yannopapas, E. Paspalakis, and N. V. Vitanov, Phys. Rev. Lett. **103**, 063602 (2009).
[24] C. Henkel, K. Joulain, R. Carminati, and J. J. Greffet, Opt. Commun. **186**, 57 (2000).
[25] R. Kolesov, B. Grotz, G. Balasubramanian, R. J. Stohr, A. A. L. Nicolet, P. R. Hemmer, F. Jelezko, and J. Wrachtrup, Nat. Phys. **5**, 470 (2009).
[26] V. V. Klimov and M. Ducloy, Phys. Rev. A **69**, 013812 (2004).
[27] Y. N. Chen, G. Y. Chen, D. S. Chuu, and T. Brandes, Phys. Rev. A **79**, 033815 (2009).
[28] D. Dzsotjan, A. S. Sorensen, and M. Fleischhauer, Phys. Rev. B **82**, 075427 (2010).
[29] H. P. Breuer, D. Faller, B. Kappler, and F. Petruccione, Phys. Rev. A **60**, 3188 (1999).
[30] F. J. Rodríguez, L. Quiroga, C. Tejedor, M. D. Martín, L. Viña, and R. André, Phys. Rev. B **78**, 035312 (2008).
[31] S. Savasta, R. Saja, O. D. Stefano, P. Denti, and F. Borghese, arXiv:1003.2394 (unpublished).
[32] H.-P. Breuer and F. Petruccione, *The Theory of Open Quantum Systems* (Oxford University Press, Oxford, 2002).
[33] S. Scheel and S. Y. Buhmann, Acta Phys. Slov. **58**, 675 (2008).
[34] P. Johnson and R. W. Christy, Phys. Rev. B **6**, 4370 (1972).
[35] M. Lewenstein and T. W. Mossberg, Phys. Rev. A **37**, 2048 (1988).
[36] A. Imamog¯lu, Phys. Rev. A **50**, 3650 (1994).
[37] P. Stenius and A. Imamoglu, Quantum Semiclassic. Opt. **8**, 283 (1996).
[38] I. Wilson-Rae and A. Imamoglu, Phys. Rev. B **65**, 235311 (2002).
[39] H. P. Breuer and B. Vacchini, Phys. Rev. Lett. **101**, 140402 (2008).
[40] X. Ma and S. John, Phys. Rev. Lett. **103**, 233601 (2009).
[41] G. Burkard, Phys. Rev. B **79**, 125317 (2009).
[42] D. Chruściński and A. Kossakowski, Phys. Rev. Lett. **104**, 070406 (2010).
[43] P. Kaer, T. R. Nielsen, P. Lodahl, A.-P. Jauho, and J. Mork, Phys. Rev. Lett. **104**, 157401 (2010).
[44] C. Roy and S. John, Phys. Rev. A **81**, 023817 (2010).
[45] P. Haikka and S. Maniscalco, Phys. Rev. A **81**, 052103 (2010).
[46] B. Vacchini and H. Breuer, Phys. Rev. A **81**, 042103 (2010).
[47] D. Walls and G. Milburn, *Quantum Optics* (Springer-Verlag, Berlin, 1994).
[48] G. Khitrova, H. M. Gibbs, M. Kira, S. W. Koch, and A. Scherer, Nat. Phys. **2**, 81 (2006).